Surfactant-enhanced heterogeneity of the aqueous interface drives water extraction into organic solvents

Journal:	*Physical Chemistry Chemical Physics*
Manuscript ID	CP-ART-10-2018-006450.R1
Article Type:	Paper
Date Submitted by the Author:	16-Nov-2018
Complete List of Authors:	Servis, Michael; Washington State University College of Arts and Sciences, Clark, Aurora; Washington State University, Chemistry

Journal Name

ARTICLE TYPE

Cite this: DOI: 10.1039/xxxxxxxxxx

Surfactant-enhanced heterogeneity of the aqueous interface drives water extraction into organic solvents†

Michael J. Servis,*[a] and Aurora E. Clark*[a]

Received Date
Accepted Date

DOI: 10.1039/xxxxxxxxxx

www.rsc.org/journalname

Liquid/liquid extraction (LLE) is one of the most industrially relevant separations methods, successfully leveraging the variable solubility of solutes (or their complexes) between two immiscible solvents. Independent of the relative solubilities of those solutes and complexes which determine their distribution between phases, the dynamics of phase transfer processes are impacted by the molecular interactions and structure of those species at the interface. A simple example includes the formation and extraction of water-extractant adducts observed in the ternary water/organic/tri-*n*-butyl phosphate (TBP) system. Despite its implications for LLE, a detailed description of the structural and dynamic mechanisms by which such adducts are formed at the interface is not established. Describing that process requires connecting the evolving interfacial molecular organization in the presence of surfactants to dynamic surface fluctuations and interfacial heterogeneity. Herein, molecular dynamics simulation is combined with state of the art network theory analysis to reveal features of interfacial structure and their relationship to the extraction of water in the water/*n*-hexane/TBP system. Surfactant adsorption enhances interfacial roughness which in turn causes directly interfacial water to become less connected through hydrogen bonding to subjacent layers, particularly upon formation of the water bridged TBP dimer adduct. Further, heterogeneity within the interface itself is enhanced by surfactant adsorption, and serves as the basis for the formation of protrusions of water into the organic phase at the extremes of surface fluctuations. These features disproportionately incorporate the water bridged TBP dimer and are the primary means by which water is transferred to the organic phase. This work presents for the first time a holistic understanding of how interfacial heterogeneity and spatial fluctuations become amplified in the presence of surfactants, enabling water extraction into the organic phase. It further affords the opportunity to study how solution conditions can control interfacial behavior to create more efficient solvent extraction systems.

1 Introduction

Industrial liquid/liquid extraction (LLE) is the primary means of metal recovery and purification applied to a wide variety of solutions that span dissolved ores in mining to spent fuel from nuclear power plants.[1] In this context, LLE generally employs ternary aqueous/organic/surfactant solutions that leverage the relative solubilities of surfactant-solute complexes between phases. While those solubilities determine the distribution of species between equilibrated phases, the extraction dynamics are dictated by the formation and subsequent extraction of surfactant-solute adducts at the liquid/liquid interface. The assembly of these complexes[2,3] represents a kinetically limiting process[1,4] occurring at an interface whose structure is significantly perturbed by the surfactant itself. This process is a challenging area of study, as experimental characterization is limited by the relatively small set of spectroscopic signatures of solvents in the interfacial region (e.g., solvent orientation by vibrational sum frequency generation spectroscopy) or to changes in features like electron density obtained from X-ray reflectivity.[5,6] Nevertheless, these works in combination with molecular simulation have informed the development of a theoretical understanding of the statistical broadening of the interfacial width due to thermal induced capillary wave fluctuations of the interface.[6,7]

Despite the potential benefits associated with employing surfactants to initiate interfacial reactivity or enhance transport,[8,9] the underlying molecular-level understanding of how a surfac-

[a] Department of Chemistry, Washington State University, Pullman, WA, USA. E-mail: michael.servis@wsu.edu
[b] Department of Chemistry, Washington State University, Pullman, WA, USA. E-mail: auclark@wsu.edu

† Electronic Supplementary Information (ESI) available. See DOI: 10.1039/b000000x/

tant perturbs capillary waves and the relationships between molecular-scale organization, macroscopic interfacial properties, and transport mechanisms are not well known. The dearth of knowledge has created a critical barrier to advancing LLE technologies.[10] Relative solubilities and structures of species between two phases can be obtained from simulation techniques including Gibbs ensemble Monte Carlo simulation.[11–13] However, to understand the species and structures which form at the interface and inform the dynamics of extraction, explicit simulation of the interface is required. In principle, interfacial organization and spatial fluctuations can be utilized as design features to control interfacial speciation and transport, creating more robust extraction gateways that increase separations efficiency. Thus, optimizing separations efficiency and moving into next generation LLE systems requires a detailed understanding of dynamic molecular organization, reactions, and transport processes at the interface itself.

The experimental challenges of measuring the structural and dynamic properties of liquid/liquid interfaces has inspired widespread use of molecular dynamics (MD) simulations.[7,14–28] Those studies often report solvent density profiles, average molecular orientation, and interfacial tension. However, it is now necessary to study how the dynamic processes of the interface are coupled to molecular structure – considering the surface heterogeneity with an instantaneous, rather than time averaged, description.[22,28–30] Among the methods used to determine an instantaneous interface from molecular simulation is the identification of truly interfacial molecules (ITIM)[26,28], which directly measures a molecule's occupation of the interfacial layer independent from its distance to the time averaged interfacial plane (e.g., the Gibbs dividing surface). This allows quantification of the interfacial roughness and its relationship to the molecular structure of the interfacial solvent molecules[22,28,31]. In this work the surfactant tri-*n*-butyl phosphate (TBP) is chosen because of its ubiquity in solvent extraction applications[1,32], notably in the Plutonium Uranium Reduction EXtraction (PUREX) process, and because it has been the topic of extensive study in the MD modeling literature[9,11,20,33–42]. Prior work[8,20,42,43] has shown that TBP adsorbs to the water/organic interface with its dipole orthogonal and alkyl tails parallel to the interface plane. While the extraction of water from the interface by TBP has been qualitatively described in the literature[8,42], it remains to be understood – either qualitatively or quantitatively – how TBP adsorption influences the capillary wave front, including its heterogeneity, fluctuations in space, and the resulting mechanisms for water extraction into the organic phase. To address these issues requires quantifying the structural features of TBP, water, and the ensemble of interfacial configurations that may be correlated to capillary wave behavior. This necessitates unique analysis, which herein combines the ITIM description of the aqueous/organic interface with chemical network analysis of TBP-water and water-water hydrogen bonding (HB) coupled to concentration dependent interfacial roughness.

This approach demonstrates how TBP adsorption affects interfacial water structure directly through hydrogen bonding. Formation of the water bridged TBP dimer adduct, TBP$(H_2O)_{1-2}$TBP, decreases the interaction of the bridging water with subjacent interfacial water. Further, TBP indirectly affects interfacial water by increasing the spatial extent of capillary wave fluctuations wherein the water bridged dimer is observed to form at the crests of the wave front. The TBP$(H_2O)_{1-2}$TBP species is indeed a common structure at the interface, whose formation relies upon the interfacial heterogeneity associated with the physical properties of capillary wave crests versus troughs. The crests of the capillary waves under high surfactant concentration become protrusions of water from the aqueous surface into the organic phase. These features serve as the primary dynamic water extraction pathway and highlight the importance of the TBP$(H_2O)_{1-2}$TBP species as demonstrated by its ubiquity during protrusion formation and as a thermodynamically favored specied at equilibrium in the bulk organic phase. A new holistic understanding that illustrates the importance of both the intrinsic capillary wave features, and the enhancement of surface roughness and heterogeneity caused by the surfactants, is thus developed that provides a driving force for the formation of the protrusions and subsequent extraction mechanism. Given that these interfacial structures form and disperse over the ns timescale, they are challenging to resolve experimentally without a prior understanding of possible structural features to probe. Therefore, the structures predicted here also serve to inform future experimental investigation into surfactant-water interfacial reactivity at liquid/liquid interfaces and develop a new chemical basis for optimizing surface conditions to minimize water-adduct formation.

2 Computational Methods

2.1 Simulation Systems and Force Fields

Classical molecular dynamics simulations were performed to study the effect of TBP concentration on the water/*n*-hexane interface. The surfactant TBP concentration traversed dilute (1 TBP per interface) to near saturation (93 available TPB for interfacial adsorption). The latter corresponds to industrial PUREX process conditions. The AMBER-based force field for TBP has been optimized by Ye et al.[42] for the interfacial water/*n*-alkane system to accurately reproduce the experimentally determined extracted water concentration in the organic phase at equilibrium[38,42]. System compositions, simulation methodology and force field descriptions are given in the Supporting Information. Additional data using alternative force fields are presented in Supporting Information and validate that key results are independent of the force field employed.

2.2 Analysis Methods

The directly interfacial water layer is composed of H_2O that are nearest neighbors of *n*-hexane solvent molecules. This, and subjacent layers, were determined instantaneously using the Identification of Truly Interfacial (ITIM) algorithm[28]. Figure 1 presents a snapshot of the 56 total TBP simulation system with three insets showing the interfacial TBP (left), and the three interfacial water layers as identified by ITIM (center). Water-water and water-TBP HB networks were determined using a graph theoretical approach with the ChemNetworks software[44], depicted schemati-

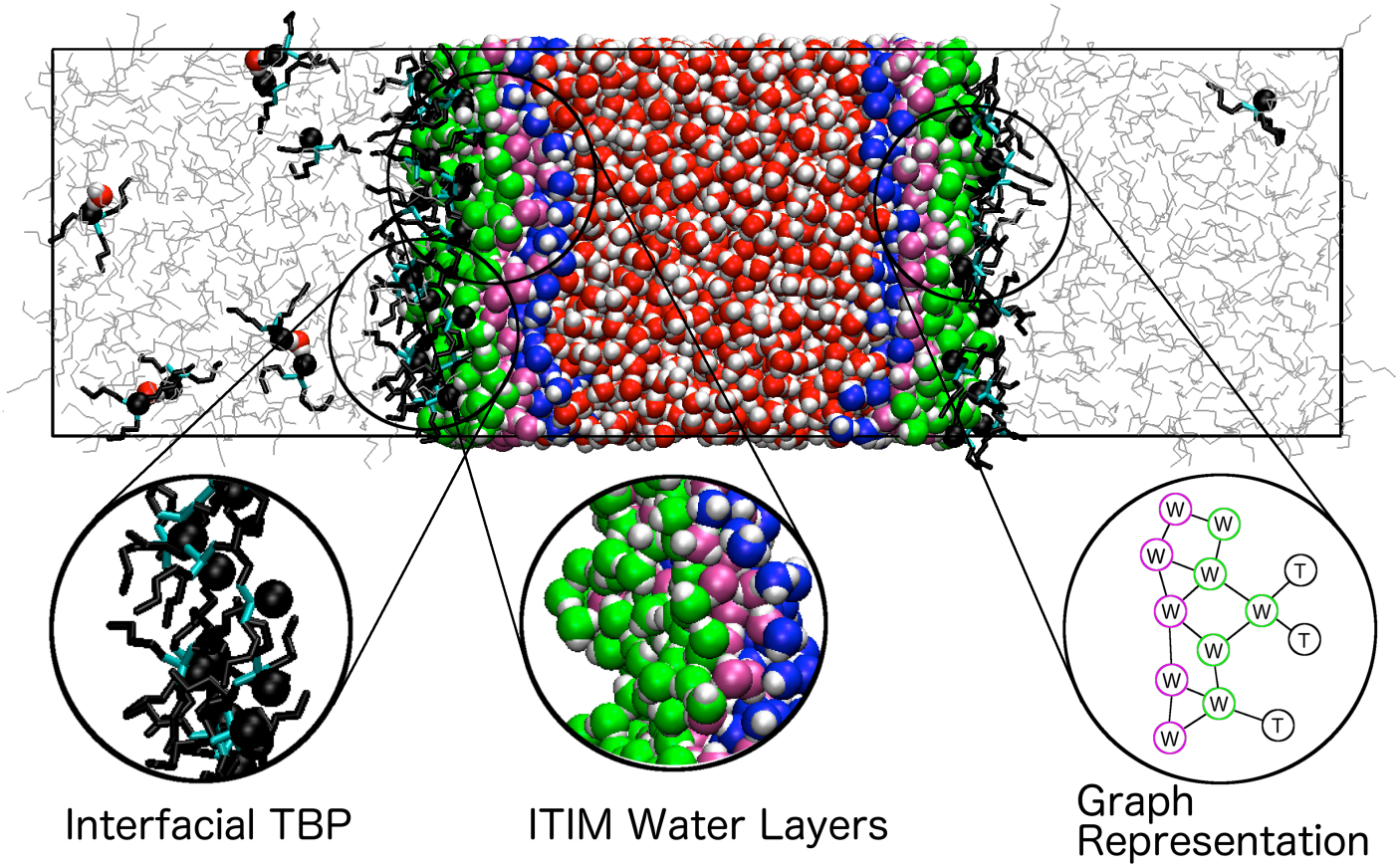

Fig. 1 The interfacial TBP (left inset), first three interfacial water layers determined by ITIM with green, purple and blue oxygens, respectively, (middle) and a graph representation of interfacial water and TBP hydrogen bonding (right) are depicted for the 56 total TBP system. Non-interfacial water are depicted in red and *n*-hexane with gray lines. The alkyl tail carbon atoms of TBP are drawn in black with cyan for the phosphate head group and the phosphoryl oxygen of the TBP highlighted in black.

cally in the right inset of Figure 1. Hydrogen bonding of water and adsorbed TBP is then coupled with ITIM layer membership and molecule z-position to interpret the relationship between surface heterogeneity, local hydrogen bonding, and intact molecular configurations that include the TBP$(H_2O)_{1-2}$TBP species. Interfacial tension calculated using the pressure tensor, molecular density profiles, time-averaged spatial distribution and orientation of the directly interfacial water layer are given in the Supporting Information. The interfacial width and Gibbs dividing surface were determined from Gaussian fits of the the time-averaged directly interfacial water z-position distributions, where the Gibbs dividing surface is the z-position where the water density is 50% of its bulk value. The Gibbs dividing surface is labeled at z = 0 in all pictorial representations. The periodic simulations necessarily contain two interfaces and the reported interfacial properties are the average. Details on these analysis methods and density profiles for each component of all the simulations are given in the Supporting Information.

3 Results

3.1 Surfactant Adsorption Increases Interfacial Roughness

The average number of interfacial TBP versus the total number available is plotted in the left panel of Figure 2. For low total TBP concentrations, nearly all of the TBP is located at the interface. At higher than 20 TBP surface loading, the surfactants begin to distribute to the bulk *n*-hexane in significant quantities as interfacial saturation is asymptotically approached. It has been previously postulated that interfacial roughness may enhance surfactant reactivity with aqueous solutes[8]. Here, the roughness is quantified by the fitted full width at half maximum of the directly interfacial water layer z-position distribution and is plotted in the right panel of Figure 2. The directly interfacial water layer distributions were well fitted by a Gaussian distribution, as described in the Supporting Information. At low interfacial TBP concentrations, adsorbed TBP are readily incorporated into the interfacial water HB network. At this point the surface tension begins to drop even though changes to the interfacial width indicate only modest enhancement of surface roughness (Figure 2). However, above the 10 TBP interfacial concentration, incorporation into the directly interfacial water network begins to cause a significant increase to the interfacial width and concomitant major decreases to the interfacial tension. Thus at TBP organic phase concentrations that are relevant to process conditions significant perturbation of the interface is observed. Note that the experimental value is 51.4 mN/m for the pure water/*n*-hexane system[45] and 8.8 for the TBP saturated water/*n*-hexane[46] interface and that the calculated val-

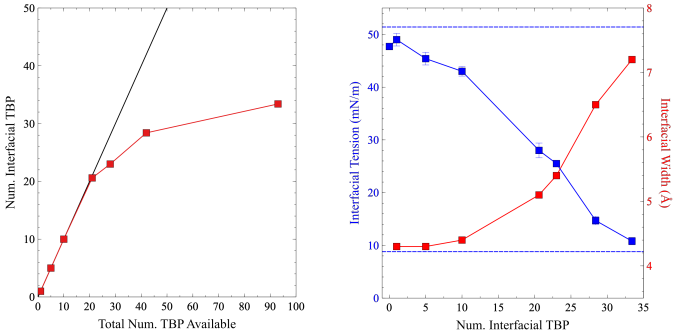

Fig. 2 In the left panel, the average number of TBP at an interface for each simulation is plotted against the total number of TBP available to adsorb from the organic phase. For reference, a line is drawn corresponding to hypothetical adsorption of all of the TBP in the simulation box. In the right panel, the average number of TBP at an interface for each simulation is plotted against the fitted width of the directly interfacial water layer in red, corresponding to the right axis. The interfacial tension is plotted with blue squares, corresponding to the left axis.

ues fall within these two limits.

3.2 Interfacial Hydrogen Bonding

The microscopic surface features of liquid/liquid interfaces, with or without adsorbed surfactant, are known to vary both dynamically and spatially across an instantaneous surface at nanoscale distances[22]. Additional surface heterogeneity, introduced by surfactant adsorption, is expected to perturb interfacial hydrogen bonding which dictates the structure and energetics of mixed surfactant/water species and informs the types of aggregates that TBP form in the interfacial region. The distribution of TBP HBs with water is plotted in Figure 3A as a function of interfacial TBP concentration. At lower interfacial concentrations, roughly 75% of TBP have 2 HBs with water while the remaining TBP population have between 1 or 3 HBs. As the concentration of TBP at the interface increases, the 2- and 3-hydrogen bond TBP populations decline while the 1-hydrogen bond TBP population increases, reducing the average connectivity of individual TBPs with directly interfacial water.

Importantly, the average HB number of TBP is affected by the position of a given TBP along the water interface capillary wave front (Figure 3B). The distribution of distances in the z-dimension between the TBP phosphoryl oxygen and the water Gibbs dividing surface as a function of TBP with different numbers of HBs with water, is plotted in Figure 3B (for the system with 28.4 interfacial TBP). A larger number of HB's with water are probable when TBP exists in a capillary wave trough, closer to the bulk water phase, because the concave form of the regions enable more waters to surround an adsorbed TBP. At the same time these interfacial waters reorient by 180 degrees from the preferred interfacial orientation upon HB formation with TBP (see Supporting Information). These perturbations to water structure are roughly proportional to the amount of adsorbed TBP present. HB statistics for the first three interfacial water layers in the absence of TBP are given in Figure S9 for comparison to existing studies of the water/hexane and other interfaces. Changes from the pure water/hexane interface to the distribution of water-water HBs for the interfacial water layer are given for each TBP concentration in Figures S10 and S12.

In addition to changes in HB structure and orientation of interfacial water, adsorbed TBP leads to additional interfacial roughness beyond those from capillary fluctuations. Enhanced roughness leads to a second, indirect, effect upon hydrogen bonding within the interface. Specifically, enhanced interfacial roughness increases water-water hydrogen bonding, specifically for those waters that are not interacting directly with TBP at all. As TBP concentration increases, H_2O that are not hydrogen bonding with TBP gain an additional 0.193 ± 0.003 HBs with other H_2O on average with error computed from 5 ns block averaging. This could result from the fact that a more planar interface (less surface roughness) strains the ability of water to form its preferred tetrahedral configuration of hydrogen bonds, and that it is easier to have 4 tetrahedrally coordinating HB neighbors when more spatial fluctuations of the interface are present. Plotted data concerning this analysis and further discussion of water-water hydrogen bonding and reorientation by TBP is included in the Supporting Information.

In combination, these data imply that surface roughness (dictated by surfactant concentration) and position of surfactant at different regions of a heterogeneous interface may impact the reactivity of that surfactant with water or aqueous solutes. At the highest TBP loading, those TBP at the troughs of the capillary wave are surrounded by more water, causing waters to reorient and also maximize their hydrogen bonding with one another, while at the crests of the capillary waves TBPs have a limited HB network with water. Although increased interfacial area has been attributed to enhancing the surface activity of TBP by providing more total area for reactions to occur[8,42], the local structure, and therefore likely the reactivity, of TBP varies as a function of the heterogeneous character within different positions in the capillary wave front and cannot be ignored (vide infra).

3.3 Interfacial TBP-TBP Correlation and the Water Bridged TBP Dimer

The spatial correlation of adsorbed TBP is measured with a 2-dimensional radial distribution function (RDF - labeled $g(r)_{TBP-TBP}$), as described in the Supporting Information, and plotted in Figure 4. Over the range of TBP concentrations considered, the radial distribution is less than unity until roughly 10 Å, with a correlation peak near 4 Å. Beyond 15 Å, interfacial TBPs are uncorrelated. The RDF is computed only between adsorbed TBP and the distances between TBP are projected onto the planar interface. Because TBP adsorb with their alkyl tails parallel to the interfacial plane, the anti-correlated region in $g(r)_{TBP-TBP}$ before the plateau observed for all TBP concentrations is attributed to the steric overlap of TBP alkyl tails within the interfacial plane which limits TBP configurations until a TBP-TBP distance of about 12Å, as depicted in Figure 4B. These data contrast with that observed for surfactants with single linear alkyl chains, such as *n*-octanol or certain sodium alkyl sulfates, which orient perpendic-

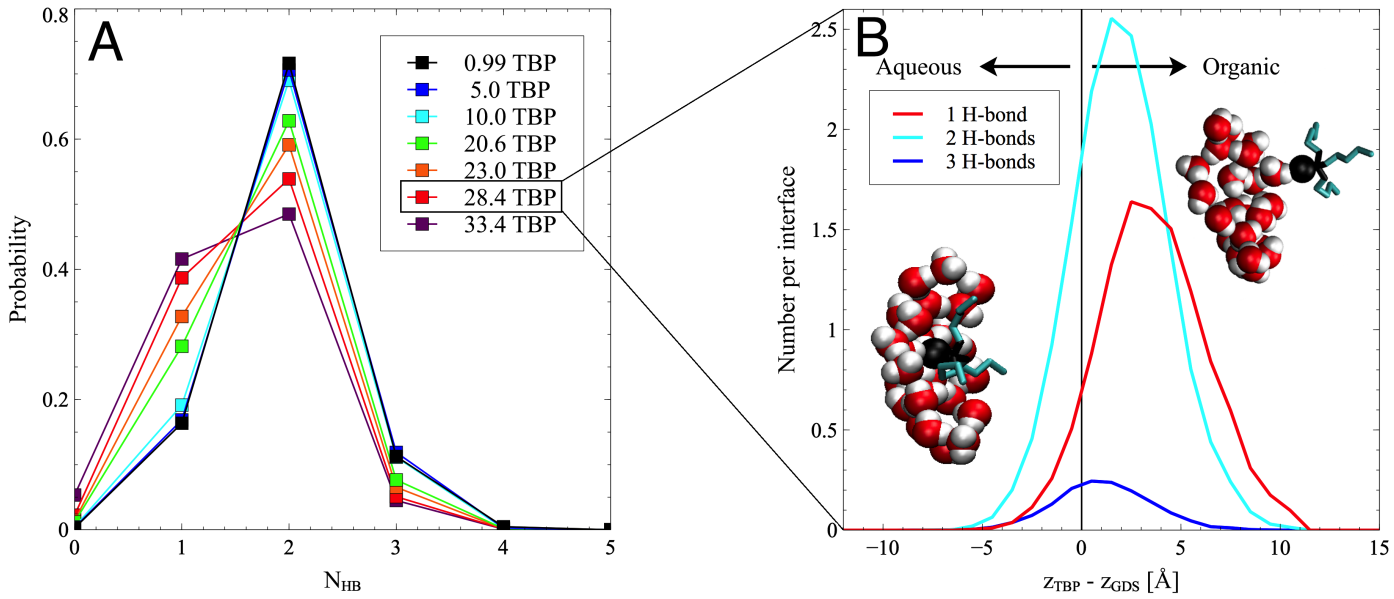

Fig. 3 The probability of participating in a given number of hydrogen bonds with water, N_{HB}, for interfacial TBP is plotted in panel A, labeled by the average number of TBP at the interface. Lines are drawn connecting data points for visual clarity. Panel B shows the distribution of TBP positions relative to the water Gibbs dividing surface for each water hydrogen bond number for that TBP. Positive values indicate TBP positions on the organic phase side of the Gibbs dividing surface. Inset are snapshots showing TBP located at capillary wave crest (positive or organic facing) and trough (negative or aqueous facing) regions of the interface.

ular to the interfacial plane and therefore likely experience different steric limitations to adsorption[47,48]. This implies that the adsorption free energy could depend on the molecular structure of the surfactant alkyl tails, including length and branching.

The $g(r)_{TBP-TBP}$ correlation peak at near 4 Å corresponds to the TBP(H_2O)TBP species, depicted in Figure 4A, where the water molecule is embedded in the directly interfacial water layer while donating hydrogen bonds to two different TBP. The extracted TBP(H_2O)TBP species has been posited by the experimental literature[49] and observed in the bulk organic phase in other simulation studies[8,11,37] and its presence at the interface implies its stability and predominant role in the transfer process of water from the interface into the bulk organic phase. The concentration of interfacial TBP(H_2O)TBP per unit of interfacial area is presented in the left panel of Figure 5 with the average z-dimension distance between the bridging water and the Gibbs dividing surface. Increased TBP concentration corresponds to increased TBP(H_2O)TBP that are located further from the bulk aqueous phase, the positive z-direction, in the capillary wave front (crests). This is accompanied by perturbations to the hydrogen bonding of the bridging H_2O in the TBP dimer adduct, as shown in the right panel of Figure 5. Two features of the hydrogen bonding were analyzed. First the bridging H_2O hydrogen bonds with other H_2O in the directly interfacial layer was studied, followed by study of the HBs of the bridging H_2O with the immediately subjacent layer. At low TBP concentrations, there are on average one HB between the bridging H_2O in TBP(H_2O)TBP and other water. As the TBP concentration increases most of the connectivity to the subjacent water layer is lost. This is illustrated schematically in the inset of Figure 5, where the TBP(H_2O)TBP on the rougher capillary wave fronts (higher TBP concentration) are less connected to the subsurface layer relative to lower TBP concentration that have smaller fluctuations in the z direction. Therefore, for systems with heightened surface heterogeneity, more TBP(H_2O)TBP form at the crests of the capillary waves and with significantly reduced connectivity to the bulk. In combination, these data indicate that the enhanced surface heterogeneity (variation between troughs and crests) encourages the formation of TBP(H_2O)TBP, a structure that is essential to separating water from the directly interfacial layer and enabling water extraction.

3.4 Dynamic Water Extraction

The most important conclusion from these data is that surface roughness coupled to the formation of the TBP(H_2O)TBP species play a central role in the dynamic process of water extraction into the bulk organic phase. The highest concentration system corresponds to process relevant conditions, and has been examined further in the context of dynamic extraction events. Four representative extraction processes are depicted in Figure 6A-D with timestamps where extracted or soon-to-be extracted water is depicted in blue and the TBPs that form organic phase clusters with those water are highlighted from other TBP that remain at the interface. Water is found to nearly always extract from the protrusion architecture although the character of those protrusions varies. In Figure 6A, two TBP extract two water, which form a TBP(H_2O)$_2$TBP cluster shortly after leaving the interface. In panels B and C, water is extracted in larger clusters with several TBP. The protrusion formed immediately before extraction in panel B is linear with the entire protrusion transferring to the organic phase. In panel C, only a portion of the protrusion is extracted by the TBP. In panel D, the largest observed extracted cluster consisting of 14 water and 6 TBP, is shown. This process

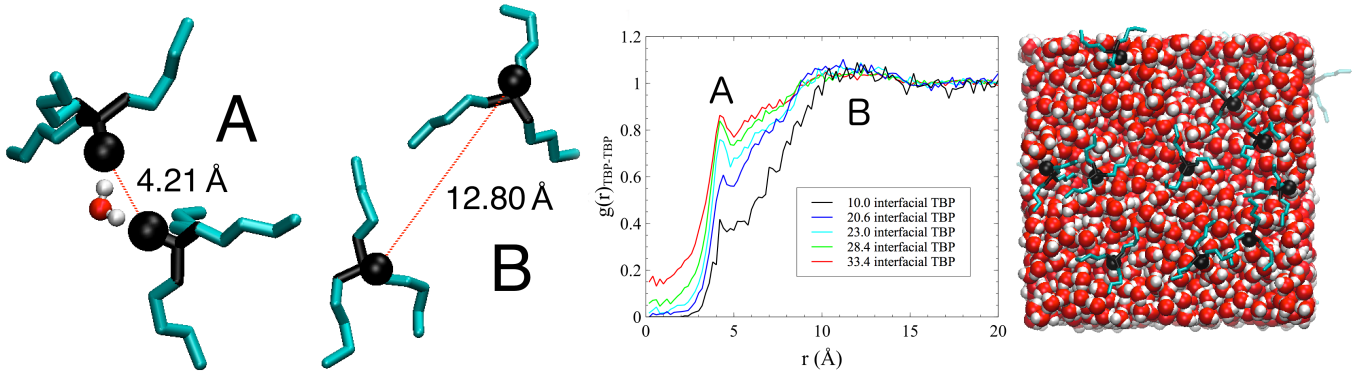

Fig. 4 Two dimensional RDFs of interfacial TBP are plotted for each system with interfacial configurations corresponding to the peak (A) and plateau (B) regions. On the right, the distribution of interfacial TBP is shown looking along the z-axis for the lower concentration 10 TBP per interface system. TBP are depicted with the phosphoryl oxygens drawn as spheres. Water is drawn in red (oxygen) and white (hydrogen) and n-hexane is not included for clarity.

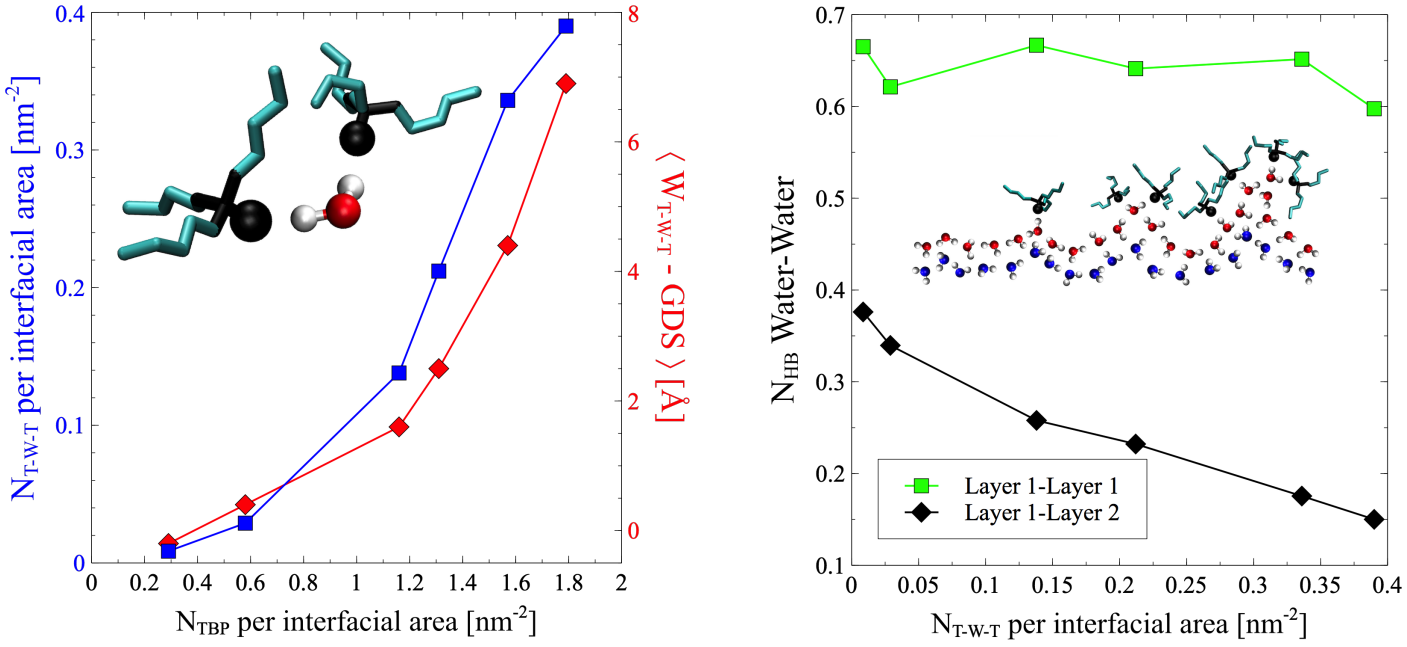

Fig. 5 Left panel: the average number of interfacial TBP(H_2O)TBP (inset, denoted T-W-T), is plotted per interfacial area (left axis) and the average z-dimension distance between the participating water and the Gibbs dividing surface (right axis), is plotted as a function of the number of TBP(H_2O)TBP per interfacial area. Right panel: the number of water-water hydrogen bonds, within the directly interfacial layer and with the subjacent layer, for the bridging water of TBP(H_2O)TBP are plotted as a function of their total number. Inset is a schematic depiction of the impact of roughness on the formation of TBP(H_2O)TBP and the reduction of hydrogen bonding of the bridging water with the subjacent layer.

in panel D resembles reverse micelle formation at the interface, with the initial protrusion (first frame, t = 21.64 ns) evolving to form a narrow neck with a single water connecting it to the bulk phase (second frame, t = 22.12 ns) before separating entirely from the aqueous interface (third frame). The final frame highlights the reverse micelle character of the extracted cluster, with TBP alkyl tails surrounding the polar core. While water is often extracted in larger clusters, they are not thermodynamically stable in the organic phase and dissociate after extraction, forming the most frequently observed TBP(H_2O)TBP species, or less often the TBP(H_2O)$_2$TBP species.

The extraction mechanisms described above convey several unique characteristics of this extraction system. More than increasing the total interfacial area, TBP saturation at the interface results in protrusions through which water extraction is possible. The examples of protrusions in Figure 6 focus upon observed extraction events, these structures form spontaneously and result in water extraction most but not all of the time. Further, the protrusions are noticeably different in curvature than typical capillary fluctuations. The surfactant induced surface perturbations to the inherent capillary roughness of a liquid-liquid interface creates distinct structural features (protrusions) that facilitate water extraction from the surface. While extracting events at lower concentrations may result in water protrusions similar to Figure 6B, reaction pathways that feature larger cluster extractions are less frequent. Throughout protrusion formation and extraction, the TBP(H_2O)TBP species is frequently observed, demonstrating that the reduction in HB connectivity to the aqueous bulk at the extremes of surface roughness facilitate pulling clusters of water from the surface into the organic phase. Interestingly, nearly all possible hydrogen bonds donor sites within the protrusion are occupied, i.e., there are few dangling O-H bonds irrespective of the size or shape of the protrusion architecture. This indicates that discrete hydrogen bonding energetics inform the specific configurations adopted by the protrusions. Lastly, it is important to note that the TBP-water cluster speciation at the “interphase" region (whether of TBP(H_2O)$_n$TBP or more complex species) can be different from the equilibrium organic phase speciation that favors TBP(H_2O)$_{1-2}$TBP. Likewise, TBP extraction of solutes aside from H_2O could similarly undergo coordination or structural changes in the interphase region.

Although formation of “fingers,” or protrusions, resulting from thermal fluctuations at the interface, and their impact on ion phase transfer have been discussed in the literature[50–61], initially apparent distinctions can be made with the observations made herein. Liang *et al.*[61] invoke curvature and line tension energetics, rather than discrete molecular interactions, to describe ion/water/extractant micelle formation at the interface. Yet in the water/*n*-hexane/TBP system, water protrusions avoid dangling O-H bonds and the resulting prevalence of TBP(H_2O)$_{1-2}$TBP structures indicate that discrete molecular interactions likely govern protrusion structure energetics instead. Further, prior observation of water protrusions that trail ions that are transferred into nitrobenzene[62], chloroform[59] or dichloromethane[51,60] organic phases often display numerous exposed hydrogen bond donor sites. Therein ion transport between phases also results from a biasing potential and the protrusions do not form spontaneously (unlike the those described in this study). The generic and impactful extraction system studied here displays essential physics that demonstrate how the interfacial organization and fluctuations in capillary waves are impacted by surfactants and the ability therein for the surfactant-water adducts to separate from subjacent water layers and migrate into the bulk organic phase.

4 Conclusions

Adsorption of TBP at the water/*n*-hexane interface was studied via MD simulation to understand the effects of surfactant upon the structural and dynamic properties of the interface and mechanisms of water extraction into the organic phase. Increased interfacial roughness, and a concomitant decrease in interfacial tension, is correlated to changes in the hydrogen bonding character of adsorbed TBP and directly interfacial water. The formation of TBP(H_2O)$_n$TBP adducts and their disengagement from the interfacial region is shown to depend upon the location along the fluctuating interface (the crests of capillary wave fronts) and is assisted by a concomitant decrease in hydrogen bonding to subjacent water layers. Surfactant adsorption further induces added fluctuations to traditional capillary wave behavior, including protrusions into the organic phase. These hydrogen bonding features are expected to be further influenced by system variables that could impact surface roughness, including organic solvent, surfactant structure and the structure and concentration of aqueous solutes. The relationship between protrusion formation, extractant-induced interfacial roughness and extractant-water speciation dependent on surface heterogeneity is essential to understanding the mechanisms of liquid/liquid interfacial transport. These results will inform future interfacial mass transport modeling and design of efficient LLE systems that can now utilize capillary wave behavior as a design principle. As an example, consider the systematic study of surfactant induced capillary wave fluctuations and subsequent data-driven selection of surfactants that minimize or maximize interfacial roughness for selective transport of surfactant adducts.

5 Acknowledgements

The research described in this paper is part of the Nuclear Process Science Initiative at Pacific Northwest National Laboratory. It was conducted under the Laboratory Directed Research and Development Program at PNNL, a multiprogram national laboratory operated by Battelle for the U.S. Department of Energy. Pacific Northwest National Laboratory is operated by Battelle Memorial Institute for the U.S. Department of Energy under contract DE-AC05-76RL01830. A portion of this research used resources from the Center for Institutional Research Computing at Washington State University, in addition to the resources of the Oak Ridge Leadership Computing Facility located in the Oak Ridge National Laboratory, which is supported by the Office of Science within the Department of Energy under Contract No. DE-AC05-00OR22725.

References

1 J. Rydberg, M. Cox, C. Musikas and G. Choppin, *Solvent Extraction Principles and Practices*, Marcel Dekker, New York,

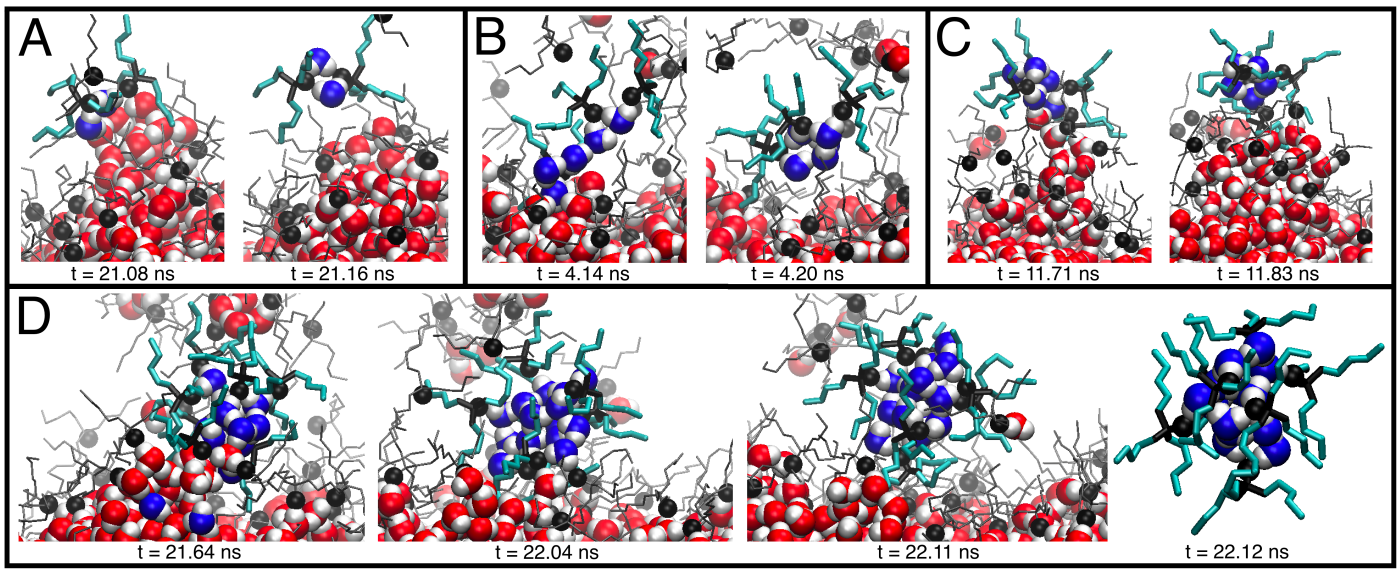

Fig. 6 Four water extraction events are depicted in panels A-D with timestamps given for each frame. Water is depicted in red (oxygen) and white (hydrogen) with oxygens of waters being extracted drawn in blue. TBP forming the extracted clusters are drawn in black (head group) and cyan (alkyl tails) while other TBP are drawn with black lines. The phosphoryl oxygen of all TBP are highlighted with spherical representations. No n-hexane is shown for clarity.

2nd edn, 2004.

2 G. Benay and G. Wipff, *J. Phys. Chem. B*, 2013, **117**, 7399–7415.

3 T. Zemb, C. Bauer, P. Bauduin, L. Belloni, C. Dejugnat, O. Diat, V. Dubois, J. Dufreche, S. Dourdain, M. Duvail, C. Larpent, F. Testard and S. Pellet-Rostaing, *Colloid. Polym. Sci.*, 2015, **293**, 1–22.

4 K. Nichols, R. Pompano, L. Li, A. Gelis and R. Ismagilov, *J. Am. Chem. Soc.*, 2011, **133**, 15721–15729.

5 A. Tikhonov, D. Mitrinovic, M. Li, Z. Huang and M. Schlossman, *J. Phys. Chem. B*, 2000, **104**, 6336–6339.

6 M. Schlossman, *Curr. Op. Coll. Int. Sci.*, 2002, **7**, 235–243.

7 A. Ismail, G. Grest and M. Stevens, *J. Chem. Phys.*, 2006, **125**, 014702.

8 M. Baaden, M. Burgard and G. Wipff, *J. Phys. Chem. B*, 2001, **105**, 11131–11141.

9 X. Ye, S. Cui, V. de Almeida, B. Hay and B. Khomami, *Phys. Chem. Chem. Phys.*, 2010, **12**, 15406–15409.

10 J. Roberto and T. Diaz de la Rubia, *JOM*, 2007, **59**, 16–19.

11 J. Mu, R. Motokawa, K. Akutsu, S. Nishitsuji and A. Masters, *J. Phys. Chem. B*, 2018, **122**, 1439–1452.

12 M. Lasich, E. Johansson and D. Ramjugernath, *Fluid Phase Equil.*, 2014, **368**, 65–71.

13 D. Harwood, C. Peters and I. Siepmann, *Fluid Phase Equil.*, 2016, **407**, 269–279.

14 H. Patel, B. Nauman and S. Garde, *J. Chem. Phys.*, 2003, **119**, 9199–9206.

15 J. Nicolas and N. de Souza, *The Journal of Chemical Physics*, 2004, **120**, 2464–2469.

16 I. Benjamin, *Ann. Rev. Phys. Chem.*, 1997, **48**, 407–451.

17 S. Patel and C. Brooks, *J. Chem. Phys.*, 2006, **124**, 204706.

18 T. Chang and L. Dang, *Chem. Rev.*, 2006, **106**, 1305–1322.

19 I. Benjamin, *J. Phys. Chem. B*, 2005, **109**, 13711–13715.

20 Y. Ghadar, P. Parmar, A. Samuels and A. Clark, *J. Chem. Phys.*, 2015, **142**, 104707.

21 J. Rivera, C. McCabe and P. Cummings, *Phys. Rev. E*, 2003, **67**, 011603.

22 T. Zhou, A. McCue, Y. Ghadar, I. Bako and A. Clark, *J. Phys. Chem. B*, 2017, **121**, 9052–9062.

23 R. Vacha, D. Horinek, M. Berkowitz and P. Jungwirth, *Phys. Chem. Chem. Phys.*, 2008, **10**, 4675–4980.

24 A. van Buuren, S. Marrink and H. Berendsen, *J. Phys. Chem.*, 1993, **97**, 9206–9212.

25 L. Dang and T. Chang, *J. Chem. Phys.*, 1997, **8149**, 8149–8159.

26 M. Sega, B. Fábián and P. Jedlovszky, *J. Chem. Phys.*, 2015, **143**, 114709.

27 P. Jedlovszky, *J. Phys: Cond. Matt.*, 2004, 5389–5402.

28 Pártay, L. and Hantal, G. and Jedlovszky, P and Vincze, Á. and Horvai, G., *J. Comp. Chem.*, 2007, **29**, 945–956.

29 E. Chacón and P. Tarazona, *Phys. Rev. Lett.*, 2003, **91**, 166103.

30 M. Jorge, G. Hantal, P. Jedlovszky and N. Cordeiro, *J. Phys. Chem. C*, 2010, **114**, 11169–11179.

31 Pártay, L. and Jedlovszky, P. and Vincze, Á. and Horvai, G., *J. Chem. Phys. B*, 2008, **112**, 5428–5438.

32 J. McKibben, *Radiochimica Acta*, 1984, **36**, 3–15.

33 Q. N. Vo, C. Hawkins, L. X. Dang, M. Nilsson and H. D. Nguyen, *J. Phys. Chem. B*, 2015, **119**, 1588–1597.

34 Q. Vo, L. Dang, M. Nilsson and H. Nguyen, *J. Phys. Chem. B*, 2016, **120**, 6985–6994.

35 M. Servis, C. Tormey, D. Wu and J. Braley, *J. Phys. Chem. B*, 2016, **120**, 2796–2806.

36 M. Servis, D. Wu and J. Shafer, *J. Mol. Liq.*, 2018, **253**, 314–325.

37 M. Servis, D. Wu and J. Braley, *Phys. Chem. Chem. Phys.*, 2017, **19**, 11326–11339.

38 J. Mu, R. Motokawa, C. Williams, K. Akutsu, S. Nishitsuji and A. Masters, *J. Phys. Chem. B*, 2016, **120**, 5183–5193.

39 A. Mondal and S. Balasubramanian, *Comp. Chem. and Mol. Sim.*, 2014, **106**, 1235–1242.

40 S. Cui, V. de Almeida, B. Hay, X. Ye and B. Khomami, *J. Phys. Chem. B*, 2012, **116**, 305–313.

41 S. Cui, V. de Almeida and B. Khomami, *J. Phys. Chem. B*, 2014, **118**, 10750–10760.

42 X. Ye, S. Cui, V. de Almeida and B. Khomami, *J. Phys. Chem. B*, 2013, **117**, 14835–14841.

43 H. Zheng, F. Wu, B. Wang and Y. Wu, *Comp. Theo. Chem.*, 2011, **970**, 66–72.

44 A. Ozkanlar and A. Clark, *J. Comp. Chem.*, 2014, **35**, 495–505.

45 A. Goebel and K. Lunkenheimer, *Langmuir*, 1997, **13**, 369–372.

46 N. Sagert, W. Lee and M. Quinn, *Can. J. Chem*, 1979, **57**, 1218–1223.

47 B. Qiao and W. Jiang, *J. Phys. Chem. C*, 2018, **1**, 687–693.

48 W. Shi and H. Guo, *J. Phys. Chem. B*, 2010, **114**, 6365–6376.

49 B. Mokili and C. Poitrenaud, *Solv. Extr. Ion Exch.*, 1995, **13**, 731–754.

50 B. Qiao, J. Muntean, M. Olvera de la Cruz and R. Ellis, *Langmuir*, 2017, **33**, 6135–6142.

51 N. Kikkawa, L. Wang and A. Morita, *J. Chem. Phys.*, 2016, **145**, 014702.

52 J. Karnes and I. Benjamin, *J. Chem. Phys.*, 2016, 014701.

53 A. Gupta, A. Chauhan and D. Kopelevich, *Phys. Rev. E*, 2008, **78**, 1–10.

54 P. Fernandes, N. Cordeiro and J. Gomes, *J. Phys. Chem. B*, 1999, **103**, 8930–8939.

55 P. Fernandes and N. Cordeiro, *J. Phys. Chem. B*, 2000, **104**, 2278–2286.

56 K. Schweighofer and I. Benjamin, *J. Phys. Chem.*, 1995, **99**, 9974–9985.

57 L. Dang, *J.Phys.Chem.B*, 1999, **103**, 8195–8200.

58 L. Dang, *J. Phys. Chem. B*, 2001, **105**, 804–809.

59 N. Kikkawa, T. Ishiyama and A. Morita, *Chem. Phys. Lett.*, 2012, 19–22.

60 N. Kikkawa, L. Wang and A. Morita, *J. Am. Chem. Soc.*, 2015, 8022–8025.

61 Z. Lian, W. Bu, K. Schweighofer, D. Walwark, J. Harvey, G. Hanlon, D. Amoanu, C. Erol, I. Benjamin and M. Schlossman, *Proc. Nat. Aca. Sci.*, 2018, 201701389.

62 J. Karnes and I. Benjamin, *J. Chem. Phys.*, 2018, 034707.